Photoinduced chiral charge density wave in TiSe$_2$

Darshana Wickramaratne [1,*] Sujan Subedi,[2] Darius H. Torchinsky,[2] G. Karapetrov,[3] and I. I. Mazin[4,5]

[1]*Center for Computational Materials Science, US Naval Research Laboratory, Washington, DC 20375, USA*
[2]*Department of Physics, Temple University, Philadelphia, Pennsylvania 19122, USA*
[3]*Department of Physics, Drexel University, Philadelphia, Pennsylvania 19104, USA*
[4]*Department of Physics and Astronomy, George Mason University, Fairfax, Virginia 22030, USA*
[5]*Quantum Science and Engineering Center, George Mason University, Fairfax, Virginia 22030, USA*

$1T$-TiSe$_2$ has been found to host a chiral charge density wave (CDW). Some studies suggest the microscopic origin of this phase is due to electron-phonon coupling while other studies suggest it is due to an excitonic insulator phase transition based on nonthermal melting of the charge density wave. First, we propose these interpretations can be reconciled if one analyzes the available experimental and theoretical data within a formal definition of what constitutes an excitonic insulator as initially proposed by Keldysh and Kopaev. Next, we present pump-probe measurements of circularly polarized optical transitions and first-principles calculations to highlight the role of elevated electronic temperatures on structural distortions to understand the nonthermal melting of the CDW phase. We also uncover a noncentrosymmetric CDW structure that explains the finite chirality of the optical transitions observed in the CDW phase of TiSe$_2$.

I. INTRODUCTION

TiSe$_2$ is claimed to exhibit signatures of two nontrivial phenomena: an excitonic insulator (EI) phase, which is a Bose condensation of excitons, and a chiral charge density wave (CDW) phase, a state where time-reversal symmetry is spontaneously broken [1–12]. This has made it the subject of extensive experimental and theoretical studies, which in turn has led to diverging opinions on the microscopic nature of this transition. Some authors have suggested that the CDW phase of TiSe$_2$ is mostly due to an excitonic insulator transition and the structural distortion follows this purely electronic transition [1,13], while other studies have argued that the CDW in TiSe$_2$ is driven by electron-phonon coupling [9,14,15]. A third point of view has suggested that the combination of exciton and phonon interactions is required to explain the CDW phase transition [16,17].

This dichotomy in viewpoints is understandable, given that there is no distinct symmetry breaking associated with an EI transition that distinguishes it from a structural phase transition. The distinction is solely in the eyes of the beholder. An often discussed litmus test for an EI transition is a gedanken experiment where the nuclei are clamped to their equilibrium positions, and the electron subsystem experiences a transition with the atomic coordinates fixed in place. This criterion neglects the interaction between ions and electrons, which is present in any material. Furthermore, this consideration has a conceptual shortcoming: it classifies any transition associated with a divergence of the one-electron dielectric response, such as the well-known Peierls transition, as an EI, even though

such transitions are not usually described as a condensation of excitons.

In this paper we will show that it is possible to reconcile these contradictory viewpoints. Our primary focus will be to provide an explanation for the finite chirality observed in the CDW phase of TiSe$_2$ and whether this is associated with the condensation of excitons or not. The article is organized as follows. In Sec. II we briefly summarize the experimental observations that have led to the conflicting viewpoints mentioned above and propose a working definition for an exciton condensate and chiral charge density wave that reconciles these phenomena. In Sec. IV we present our pump-probe experiments and first-principles calculations that demonstrate the chiral CDW, can be explained by accounting for structural distortions that are screened by the large electronic temperature that occurs in such pump-probe studies. In particular, our working definition of an EI that we present in Sec. II B and our results in Sec. IV show that (1) the chiral CDW in TiSe$_2$ is not due to a transition to an EI phase and (2) the chiral optical transitions observed in pump-probe studies are consistent with a transition of the centrosymmetric $(2 \times 2 \times 2)$ structure to a noncentrosymmetric $(2 \times 2 \times 1)$ structure, where these two structures are near-degenerate in energy based on our first-principles calculations.

II. GENERAL CONSIDERATIONS

A. Summary of prior experimental studies

Pump-probe optical measurements are often used to address the question of whether the CDW transition is driven by an instability in the electronic or ionic response. In such experiments one can heat the electron subsystem rapidly, and probe a combination of hot electrons and cold ions. Recently this method was applied to another putative EI, Ta$_2$NiSe$_5$

*darshana.wickramaratne@nrl.navy.mil

[18], where it was conclusively shown that the gap opening is driven primarily by structural distortions. Numerous attempts to use similar spectroscopic techniques on $TiSe_2$ [2,11,19,20] have also been reported. Time-resolved x-ray diffraction (XRD) measurements or measurements of coherent phonon oscillations [2,19,20] performed during these pump-probe studies have shown the structural distortion associated with the CDW can be quenched as a function of increasing laser fluence at lattice temperatures that are well below T_{CDW}. Hence, it was conjectured that since this transition is driven by increasing laser fluence, this purportedly passes the test for $TiSe_2$ being an EI. Furthermore, plasmon softening [1] has been measured at T_{CDW} and was used as further evidence to support the EI nature of the transition. However, we will show that these assumptions are tenuous.

The observation of chiral optical transitions at lattice temperatures below the CDW transition temperature, T_{CDW}, of 200 K is another piece of intrigue around $TiSe_2$, albeit not directly related with the putative EI physics. While the original reports of static chirality in $TiSe_2$ [11] have been rebuffed [21–25], the possibility and origin of a transient chiral phase induced by photoexcitation remains an open and intriguing question [3,11].

For example, Xu *et al.* [3] observed evidence of a chiral CDW at and below 174 K through measurements of the circular photogalvanic effect (CPGE) current. This finite CPGE signal occurs at a a slightly lower temperature than T_{CDW}, which they attributed to a "gyrotropic phase" with a yet-to-be-determined noncentrosymmetric structure that is distinct from the centrosymmetric $(2 \times 2 \times 2)$ commensurate CDW phase. The CPGE is a second-order nonlinear optical effect that is described by a third-rank tensor that takes on a finite value when inversion symmetry is broken [26]. To first order with respect to an electric field, we will show this is equivalent to the off-diagonal components of the dielectric tensor becoming finite for a hexagonal material such as $TiSe_2$. However, one key assumption within the study of Xu *et al.* [3] is that the underlying atomic structure in the CDW phase already has preexisting chiral domains prior to photoexcitation. In contrast, we will show that for the case of pump-probe studies performed using high fluence, the CDW structure can take on a noncentrosymmetric structure up to a critical value of T_e. Furthermore, at a critical laser fluence and at a lattice temperature that is below T_{CDW}, the CDW and the finite chirality of the CDW spectral response is quenched [19], which has been interpreted as a nonthermal melting of the CDW phase.

B. What's in a name?

To interpret these experimental observations, it is instructive to first consider a working definition for these two phenomena; i.e., what is an *excitonic insulator* and what is a *chiral charge density wave*? When the term *excitonic insulator* [27] was first introduced, it was emphasized that the EI is an analogue of BCS superconductivity where the instability occurs in the electron-hole (e-h) rather than the electron-electron (e-e) channel. Within this definition, one would need to invoke higher-order interactions, such as ladder ("Cooper") diagrams of the Coulomb interaction to theoretically describe an EI phase. These ladder diagrams are not present in standard density functional theory (DFT) or in its Hartree-Fock-like modifications. Hence, the advantage of this definition is that it provides means to directly test whether a material should be classified as an EI based on the ability for standard DFT to describe the physical observables associated with such a phase. Note that while any failure of DFT does not imply evidence of an EI state, the phenomena associated with an EI cannot be described by standard DFT.

For the case of $TiSe_2$ this includes a simultaneous description of the $(2 \times 2 \times 2)$ reconstruction of the lattice in the CDW phase, the opening of a gap, the observation of plasmon softening at the CDW transition [1], and nonthermal melting of the CDW in pump-probe measurements at a lattice temperature well below the CDW transition temperature [2,19,28]. Hellgren *et al.* [5] demonstrated that hybrid functional DFT calculations, which do not account for electron-hole ladder diagrams, are able to reproduce the observed $(2 \times 2 \times 2)$ commensurate CDW structure and to describe the insulating state of $TiSe_2$. The plasmon softening [1] and the insulating state observed in photoemission measurements [10] are both reproduced within DFT calculations without invoking the role of excitons [5,29].

Within the EI interpretation, it is assumed that the transition occurs entirely within the electronic subsystem, while the ions follow the electronic CDW. While this line of reasoning may seem compelling, one needs to consider the fact that the ion-ion interaction is screened by electrons, and the response of the electrons may (but does not have to) depend on the electronic temperature, and thus can weaken or eliminate an ionic instability. If this mechanism is operative, the CDW disappears simply because hot electrons in a narrow-gap semiconductor, or in a semimetal, screen better than cold electrons, and therefore suppresses the magnitude of the ion-ion interaction responsible for the instability. This effect is not related to the notion of an EI. In this paper, we will show that the structural transition due to nonthermal melting has a simple one-electron explanation. Hence, nonthermal melting of the CDW structure is insufficient evidence for the presence of an EI phase.

Regarding the *chirality* of the CDW phase, a crystal structure is chiral if it can be distinguished from its mirror image; that is, the latter cannot be superimposed onto the original structure by any sequence of rotations or translations [30]. The unit cell of bulk $TiSe_2$ is composed of a single monolayer of $TiSe_2$, which leads to a centrosymmetric structure in the high-temperature phase [31]. In the $(2 \times 2 \times 2)$ CDW phase, the displacements of the Ti and Se atoms alternate between each monolayer, so that the sign of the chirality ("handedness") alternates and the $(2 \times 2 \times 2)$ CDW structure is also achiral. Hence, what is known about the $TiSe_2$ structure makes it difficult to reconcile with the observation of a chiral CDW phase. However, these considerations do not preclude the occurrence of symmetry-breaking structural distortions of the Ti and/or Se atoms that would lead to a noncentrosymmetric structure.

For the purpose of this paper we will define a chiral CDW as a structure that breaks inversion symmetry, and upon including spin-orbit coupling (SOC), leads to a combination of broken inversion and time-reversal symmetry and, in turn, nonzero optical chirality. Formally, the observation of finite optical chirality does not have to be necessarily related to

breaking of spatial symmetry breaking. For instance, one can imagine, theoretically, a situation when a finite magnetization is generated by optical pumping (even though it is rather unlikely in this material). Obviously—and consistent with the experiments that have been conducted—in $TiSe_2$ it is highly unlikely, particularly given that the effect appears only upon heating up the electronic subsystem.

III. METHODS

A. First-principles calculations

Our calculations are based on density functional theory within the projector-augmented wave (PAW) method [32] as implemented in the Vienna *Ab initio* Simulation Package (VASP) [33,34]. All of the results in the main text use the generalized gradient approximation (GGA) defined by the Perdew-Burke-Ernzerhof functional [35]. We use the Ti PAWs where the $3d$, $4s$, $4p$ and the Se PAWs where the $4s$, $4p$ electrons are treated as valence and a plane-wave energy cutoff of 400 eV. All of the structural relaxations of the bulk unit cell used a $(24 \times 24 \times 12)$ k-point grid. Calculations of the $(2 \times 2 \times 2)$ and the $(2 \times 2 \times 1)$ CDW structures used k-point grids that were scaled with respect to the k-point grid used for the unit cell. We verified that this choice in k-point grid density leads to converged results for the lowest value of smearing that we used in our calculations. An energy convergence criteria of 10^{-8} eV and a force convergence criteria of 2 meV/Å was used for all of the calculations. To examine the structural phase transition as a function of electronic temperature we used the Fermi-Dirac smearing scheme. The Grimme-D3 correction scheme was used to account for van der Waals interactions [36]. The space groups of the different structures were determined using spglib [37]. To determine the circular polarization of the optical transitions, we calculate the imaginary and real part of the dielectric function with spin-orbit interaction included within the GGA.

B. Pump-probe measurements

The optical source used here was a regeneratively amplified Ti:sapphire laser (Coherent, Astrella) producing 1.2 mJ pulses of 35 fs duration at a repetition rate of 5 kHz. A small portion of the 800 nm laser output was split off of the main beam, attenuated using reflective neutral density filters, and focused onto the sample using a 250 mm lens (Thorlabs, LA1301-A) to serve as a 0.11 mJ/cm^2 fluence excitation beam. The rest of the laser output seeded an optical parametric amplifier (Light Conversion, TOPAS Twins) that was used to produce the 620 nm (2.0 eV) and 680 nm (1.8 eV) probe wavelengths used.

A portion of the probe beam was split off before the sample to serve as a reference in order to mitigate laser noise using balanced detection, while the rest was used to measure the time-resolved circular dichroism (TRCD) signal. The probe beam polarization was converted to either left or right circular polarization by a $\lambda/4$ wave plate (Thorlabs, AQWP05M-600) and then focused onto the sample at a 45° angle of incidence using the same lens as the pump. After reflecting from the sample, the probe beam then passed through a wire grid polarizer (Thorlabs, WP25L-UB) that selected for the vertical

polarization, purified in wavelength by two longpass filters for 700 nm (Thorlabs, FESH0700) and one shortpass filter for 600 nm wavelength (Thorlabs, FELH0600) to eliminate pump scatter, and then measured by a photodiode. Data for each optical helicity were recorded as a function of mechanical delay of the pump beam and subtracted from one another to yield the TRCD signal. All data were acquired using a data acquisition card-based method described in the literature [38].

A freshly cleaved sample was glued onto a copper plate using a vacuum compatible grease (M&I Materials, Apiezon N) that was placed on a cold finger inside a closed-cycle cryostat (Montana Instruments, Cryostation 2) and then cooled down to ~6 K. Data were taken on warming in steps of ~50 K after waiting for the temperature to stabilize to within 90 mK of the target set point. Data using 620 nm and 680 nm probe wavelengths were taken on separate cool-down cycles.

IV. RESULTS AND DISCUSSION

A. Pump-probe measurements

Our measurements [39] on the picosecond timescale of the transient circular dichroism (TRCD) signal measured at 680 nm at temperatures above and below T_{CDW} are illustrated in Fig. 1(a). We find the TRCD is zero at temperatures above T_{CDW}, as expected for the achiral high-temperature phase. However, below T_{CDW} we find the TRCD takes on a finite value that is negative when our measurements are conducted with a probe wavelength of 680 nm. We also measure the TRCD at two different probe wavelengths, 620 nm and 680 nm at $T = 7.6$ K and $T = 6$ K, respectively. These measurements which are illustrated in Fig. 1(b) show that $TiSe_2$ exhibits finite optical chirality that is sign-changing. At ~7 K (well below $T_{CDW} \sim 200$ K) the TRCD is positive for measurements at 620 nm and is negative for measurements at 680 nm. This sign-changing nature of the TRCD and the wavelengths where the chirality is positive and negative are consistent with prior measurements of the spectral dependence of the TRCD [28]. At a lattice temperature of ~7 K, $TiSe_2$ is expected to take on the centrosymmetric $P\bar{3}c1$ structure which should not lead to finite chirality. The observation of finite chirality in our experiments and prior studies of $TiSe_2$ [3,11,25] raises several interesting questions.

Let us first consider a phenomenological description of the transient response upon photoexcitation in these pump-probe studies. The laser pump excites electrons to a higher energy where the energy is equal to the photon energy of the pump laser. Within a short timescale (femtoseconds) the photoexcited electrons thermalize via electron-electron interactions, which in turn raises the electronic temperature, T_e, of the electronic subsystem while the lattice temperature remains approximately fixed. Increasing the laser fluence raises T_e. Thermalization with the lattice occurs via the emission of optical phonons [40], which occurs typically on the picosecond timescale. Let us estimate what the value of T_e is based on the experiments conducted on $TiSe_2$.

For a given photon fluence, P, material volume, V, penetration depth of the excitation, l, electronic specific heat per formula unit, C_e, and reflectivity, R, the critical electronic temperature is defined as $T_e = (1 - R)PV/(lC_e)$. The
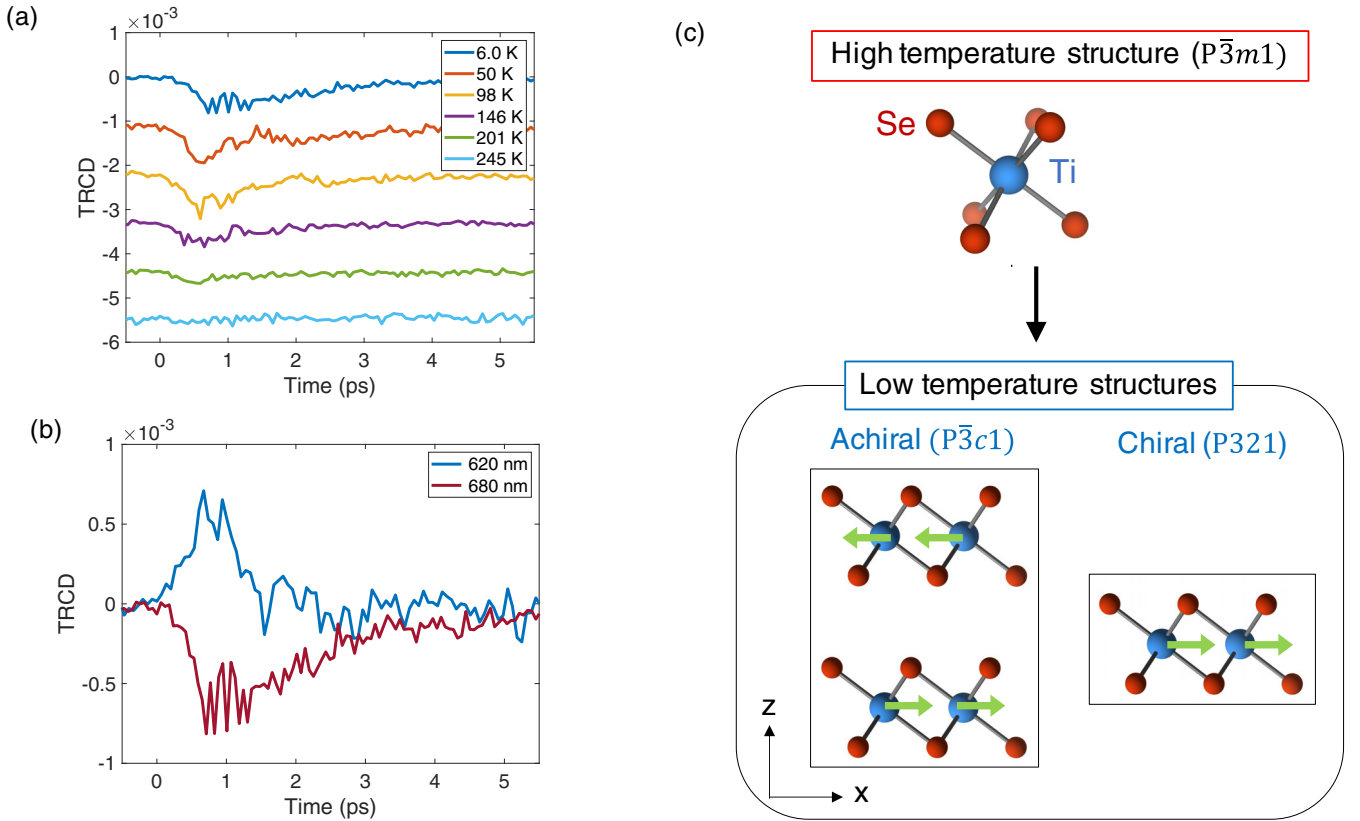
(a)

(b)

(c)

FIG. 1. Transient circular dichroism (TRCD) where $TRCD = R_t^r(\lambda) - R_t^l(\lambda)$ measured on the picosecond timescale (a) as a function of temperature using a 680 nm probe wavelength and (b) measured at $T = 7.6$ K for 620 nm probe and $T = 6.0$ K for 680 nm probe. (c) Schematic depiction of how the achiral centrosymmetric high-temperature $P\bar{3}m1$ structure can transform into either the achiral centrosymmetric $P\bar{3}c1$ CDW structure or the chiral noncentrosymmetric $P321$ CDW structure as the temperature, T, is lowered below the CDW transition temperature. The green arrows indicate the direction that the Ti atoms are displaced in the CDW phase.

average electronic specific heat, C_e, when the $TiSe_2$ charge carriers are heated from an electronic temperature of 0 K to T_e K is defined as $\frac{\pi^2}{3T}N\int_0^{T_e} T\,dT = \frac{\pi^2 NT_e}{6}$, where N is the average electronic density of states per formula unit at the Fermi level. We now use the parameters from our experiments and material-dependent properties of $TiSe_2$ to determine the change in T_e as a function of pump fluence. The results in Fig. 1 are based on an excitation wavelength, λ, of 800 nm. The absorption index, κ, at this wavelength is $\sim$3.2 [41,42]. The penetration depth, l, which is defined as $\lambda/(4\pi\kappa)$, is 19 nm for $\lambda = 800$ nm. Using the density of states at the Fermi level of $\sim$1 state/eV per formula unit, from our first-principles calculation, we find $C_e \sim 2.36T_e$. The volume of the $TiSe_2$ unit cell is 0.072 nm^3 and the reflectivity, R, at $\lambda = 800$ nm is $\sim$0.5 [43]. The magnitude of the fluence, P, used in the pump-probe studies of $TiSe_2$ ranges from 0.11 mJ/cm^2, which we use in our experiments in Fig. 1, to 0.5 mJ/cm^2 [2,19,28]. This leads to a range of values for T_e, the lowest value being $\sim$560 K and the highest value is $\sim$1200 K.

B. First-principles calculations

To elucidate whether these structural distortions are impacted by the elevated electronic temperatures that occur in pump-probe studies, we performed DFT calculations, varying the magnitude of the electronic temperature, $\sigma = kT_e$, from 0.005 eV to 0.1 eV (corresponding to an effective T_e of $\sim$58 K to $\sim$1160 K) and optimize the atomic coordinates of $TiSe_2$ using both $(2 \times 2 \times 1)$ and $(2 \times 2 \times 2)$ reconstructions. Within this approach we assume the photoexcited electrons in the pump-probe study have thermalized (within femtoseconds) to an electronic temperature that is determined in part by the fluence while the lattice temperature remains fixed. In practice, this is done by varying the magnitude of the Fermi-Dirac energy broadening, σ, used in the self-consistent cycle of our DFT calculations [39].

Above the CDW transition temperature, bulk $1T$-$TiSe_2$ is stable in a hexagonal centrosymmetric structure (space group 164, $P\bar{3}m1$) where the Ti atoms are octahedrally coordinated by Se. We use the experimental lattice constants of bulk $TiSe_2$ in the normal phase ($a = 3.527$ Å and $c = 5.994$ Å) [31] to determine the electronic structure. Our results and discussion remain unchanged if we use the lattice parameters ($a = 3.524$ Å and $c = 5.994$ Å) which we obtained by optimizing the $TiSe_2$ unit cell using the GGA functional with the Grimme-D3 correction to account van der Waals interactions [39]. We find the high-T phase to be a semimetal, with a hole-like pocket at Γ and an electron-like pocket at M and L [39]. Recall that the phonon dispersion for $TiSe_2$ [5] exhibits two soft modes, one at the M and a second at the L high-symmetry points, which correspond to structural instabilities. Indeed, the soft mode at the L point corresponds to the $(2 \times 2 \times 2)$ CDW
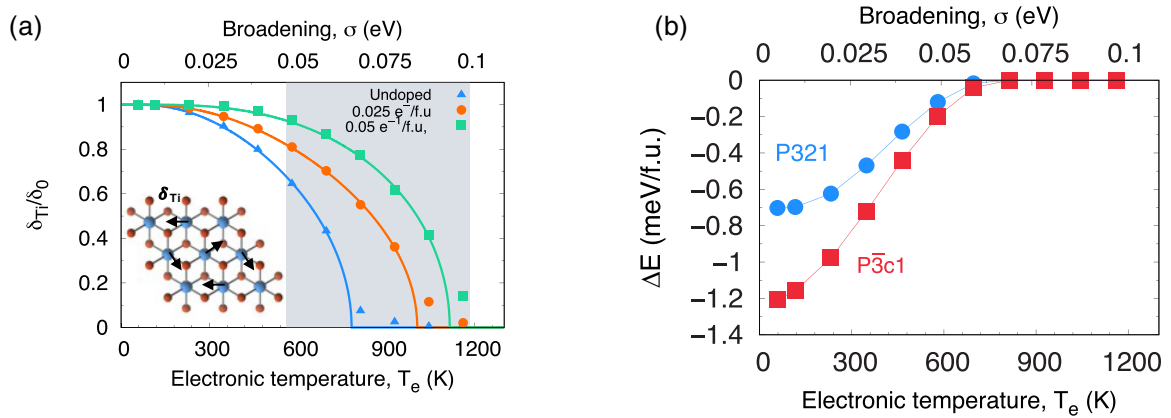
FIG. 2. Displacement of the Ti atoms in the $P321$ structure normalized by the displacement at the lowest value of T_e, as a function of T_e. Results for undoped (blue, △), and doping with 0.025 e^-/f.u. (orange, ○) and 0.05 e^-/f.u. (green, □) are illustrated. The solid lines are a fit to Eq. (1). The critical temperature, T_c, where the structure transforms to $P\bar{3}m1$ from $P321$ is the value of T_e when the solid line intersects the horizontal axis for each fit. The range of critical electronic temperatures where the chirality of the CDW is found to be suppressed in pump-probe experiments is illustrated with the gray shaded rectangle. A top view of the $P321$ structure is illustrated in the inset with the arrows illustrating the direction in which the Ti atoms are displaced. We also determine the change in the space group using Ref. [37] for each structure as a function of the electronic temperature and find the structure transforms from the chiral $P321$ space group to the high-temperature achiral $P\bar{3}m1$ space group at the same temperature as our analysis above. (b) Change in the energy difference between low-temperature and high-temperature structures as a function of electronic temperature. Data are for the achiral $P\bar{3}c1$ (□) and chiral $P321$ (○) with respect to the total energy of the high-temperature $P\bar{3}m1$ structure. The total energies at each electronic temperature reflect the displacement of the Ti and the Se atoms involved in the charge density wave.

reconstruction, which is accompanied by a displacement of the Ti along the basal plane and a minor rotation of the Se atoms around each Ti atom [31], and the corresponding space group of the structure changes from $P\bar{3}m1$ to $P\bar{3}c1$. Recent studies [44,45] have also suggested that displacements of the Ti and Se atoms are distinct from the $P\bar{3}c1$ structure. Within our DFT calculations, we find each of these displacement patterns of the Ti and Se atoms within the $(2 \times 2 \times 2)$ reconstruction to be near-degenerate in energy with respect to each other. More importantly, all these structures are centrosymmetric, similar to the $P\bar{3}m1$ unreconstructed structure or the $P\bar{3}c1$ CDW structure.

The soft mode at the M point would correspond to a $(2 \times 2 \times 1)$ structural distortion. Such a structure, which has a lower space group, $P321$, does not possess a center of inversion. Figure 1(c) illustrates these two possible structural distortions that can occur starting from the high-temperature $P\bar{3}m1$ structure.

We consider the role of an elevated T_e on the $(2 \times 2 \times 2)$ and $(2 \times 2 \times 1)$ CDW reconstructions. For each value of σ, we perform a structural optimization and determine the distance, δ_{Ti}, by which the Ti atoms are displaced away from their positions within the $P\bar{3}m1$ structure. In agreement with published results [5], we find the $(2 \times 2 \times 2)$ to be the ground state, and the magnitude of the displacement, δ_{Ti}, to be somewhat underestimated compared to experiment (it was shown in Ref. [5] that this may be corrected by adding a small fraction of Hartree-Fock exchange using a hybrid functional). The normalized displacements with respect to the displacement determined for the lowest energy broadening ($\sigma = 0.005$ eV, $T_e = 58$ K), δ_0, are shown in Fig. 2(a) for the $P321$ structure.

We find that for low values of σ, the Ti atoms are displaced strongly away from their corresponding high-symmetry po-

sition and the structure retains the low-symmetry $P321$ structure. However, at a critical value of the electronic temperature, $T_e = T_c$, the Ti atoms converge to their high-symmetry positions and the structure is stable in the undistorted $P\bar{3}m1$ structure. We plot δ_{Ti}/δ_0, which we define as the order parameter for this structural transition as a function T_e and find that it exhibits a BCS-like temperature dependence. If we fit our first-principles calculations in Fig. 2(a) to the following BCS expression,

$$\frac{\delta(T)}{\delta_0} = \tanh\left(b\sqrt{\frac{1}{T} - 1}\right),$$ (1)

we find a critical temperature, T_c, to be 782 K, at which the noncentrosymmetric $P321$ structure transforms to the high-temperature centrosymmetric $P\bar{3}m1$ structure (with a Hartree-Fock correction added as in Ref. [5], this temperature would likely be slightly higher).

We also consider the effect that doping may have on this structural phase boundary. Several studies have shown as-grown $TiSe_2$ exhibits n-type conductivity that is likely due to unintentional impurities or native defects [46–48], which act as a source of excess electrons. To this end, we simulate the effect of n-type doping by changing the number of valence electrons and adding a compensating jellium background charge, and optimize the atomic coordinates and the volume starting from the $P321$ structure for different values of σ. We investigate the effect of the following doping concentrations: 0.025 e^-/$TiSe_2$ f.u., 0.05 e^-/$TiSe_2$ f.u. The change in δ_{Ti}/δ_0 as a function of σ with respect to doping is also illustrated in Fig. 2(a). We fit the results of $\frac{\delta_{Ti}}{\delta_0}$ for the two different doping levels to Eq. (1) and find T_c increases to 1005 K for 0.025 e^-/$TiSe_2$ f.u. and T_c is 1115 K for a doping concentration of 0.05 e^-/$TiSe_2$ f.u.

We also conducted a similar analysis as in Fig. 2(a), taking into account different approximations within DFT [39] and find qualitatively similar behavior. The order parameter always exhibits a similar BCS-like temperature dependence, and the T_c obtained by fitting $\frac{\delta_{Ti}}{\delta_0}$ versus T_e to Eq. (1) for the different approximations we tested is within 6% of the T_c for undoped TiSe$_2$ reported in Fig. 2(a).

We also explored the possibility that this transition might occur entirely within the electronic subsystem by a reduction in the symmetry of the spatial distribution of the charge density by keeping the lattice fixed and varying the electronic temperature. However, we did not observe any changes in the symmetry, which highlights the importance of allowing for symmetry-breaking lattice distortions to describe this transition. This is also consistent with the fact that even in a quintessential Peierls system, such as a one-dimensional chain of sodium atoms, DFT calculations fail to break the translation symmetry [49].

Applying the same procedure to the centrosymmetric $P\bar{3}c1$ CDW structure, we find it also converges to the $P\bar{3}m1$ structure at large values of T_e [39]. This is also reflected in our calculations of the difference in the total energy of the $P321$ and $P\bar{3}c1$ structures with respect to $P\bar{3}m1$ structure as a function of T_e, as illustrated in Fig. 2(b). The $P\bar{3}c1$ structure remains slightly lower in energy than the $P321$ structure for all values of T_e, within our static lattice calculations. The largest energy difference is 0.5 meV/TiSe$_2$ formula unit, which occurs at the lowest value of T_e that we consider. We conducted similar calculations using the HSE06 hybrid functional [39]. We find the $P\bar{3}c1$ structure remains slightly lower in energy than the $P321$ for all values of T_e. The maximum energy difference is low (-1.2 meV/TiSe$_2$ formula unit) and it occurs for the lowest value of T_e that we consider. However, this difference in energies is very small and may be reversed at some value of T_e, once the effects of vibrational entropy are properly accounted for. We speculate that this happens at some electronic temperature, T_1, such that $0 < T_1 < T_c$.

With these considerations in mind, we propose the following model to interpret the observation of nonthermal melting and the finite chirality of optical transitions that occurs for a finite range of laser fluence. While the centrosymmetric $P\bar{3}c1$ structure is the ground state CDW phase, the noncentrosymmetric $P321$ structure is near-degenerate in energy. Hence, upon photoexcitation, the rapid increase in T_e stabilizes the $P321$ structure when T_e becomes larger than T_1, and the magnitude of the displacement of the Ti atoms with respect to the $P\bar{3}m1$ structure depends on T_e. The $P321$ structure lacks a center of inversion and this, as we will show below, leads to finite circular dichroism, i.e., a chiral CDW. When T_e increases due to increasing fluence, the Ti atoms are weakly displaced with respect to their positions within the $P\bar{3}m1$ structure. At $T > T_c$, the ion-electron interactions are sufficiently weak so that the transition to the noncentrosymmetric $P321$ or the centrosymmetric $P\bar{3}c1$ structure no longer occurs. Instead, the achiral centrosymmetric $P\bar{3}m1$ structure is stable and the finite circular polarization is quenched; i.e., nonthermal melting of the (chiral) CDW occurs.

Our estimate for the critical electronic temperature, T_c, from our first-principles calculations, where the chiral $P321$ structure is quenched, ranges between 730 K
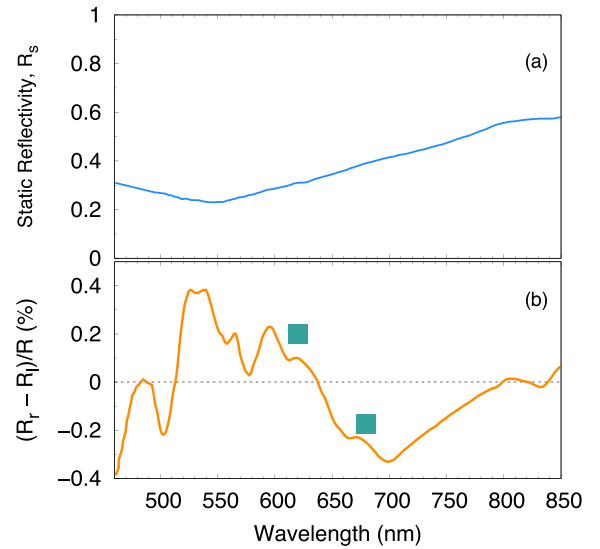

FIG. 3. (a) Total static reflectivity, R_s, of the $P321$ CDW structure as a function of wavelength. (b) Degree of chirality $[(R_r - R_l)/R_s$, where R_r corresponds to right circularly polarized reflectivity and R_l to left circularly polarized reflectivity] as a function of of photon wavelength calculated for the noncentrosymmetric $P321$ structure. The two teal markers ($\square$) denote the maximal experimentally observed chirality [Fig. 1(b)] at 620 nm and 680 nm.

for undoped TiSe$_2$ up to 1115 K for TiSe$_2$ doped with 0.05 e^-/TiSe$_2$ f.u., which is well within the range of values for the critical T_e that we estimate by analyzing the pump-probe experiments. Hence, our calculations demonstrate that the nonthermal structural transition from the CDW phase to the high-temperature phase can be described by considering the effect of an elevated electronic temperature on the structural relaxation of TiSe$_2$. Within our proposed explanation there is no need to invoke the role of excitons. The next test is whether we can explain the finite optical chirality seen in the CDW phase.

To demonstrate that the centrosymmetric $P\bar{3}c1$ and the noncentrosymmetric $P321$ structures do indeed lead to zero and nonzero chirality in their optical transitions, respectively, we calculate the real and imaginary parts of the dielectric function. We then calculate the static reflectivity, R_s, and the degree of chirality, $(R_r - R_l)/R_s$, where R_r corresponds to right circularly polarized reflectivity and R_l to left circularly polarized reflectivity [39]. The calculated reflectivity and degree of chirality are illustrated in Fig. 3.

First, we find the magnitude of the total reflectivity does not vary significantly for either the $P\bar{3}c1$ or the $P321$ CDW structures or the high-temperature $P\bar{3}m1$ structure. For photon wavelengths between 450 nm and 850 nm, the magnitude of the reflectivity ranges between ~ 0.2 and ~ 0.4. The reflectivity for the $P321$ structure is illustrated in Fig. 3(a). We note that magnitude of the reflectivity across this range of energies is also consistent with prior experiments [43].

To determine the degree of chirality we calculate the off-diagonal component of the imaginary part of the dielectric function ([39]). Since the high-temperature $P\bar{3}m1$ structure and the $P\bar{3}c1$ CDW structure both possess a center of inversion and they also preserve time-reversal symmetry, left

and right circularly polarized optical transitions are equal in magnitude and, as a result, one would expect the degree of circular dichroism to be zero. Indeed, we find this to be the case from our first-principles calculations for the two centrosymmetric structures; i.e., they are achiral.

However, for the noncentrosymmetric $P321$ structure, we find the off-diagonal components of the dielectric function are finite and this leads to finite circular polarization as we show in Fig. 3(b). There are several experimental factors that make it challenging to make quantitative comparisons between the magnitude of the experimental transient reflectivity (Fig. 1) and calculations of static reflectivity. However, we note the following two observations that emerge from our theory that are consistent with the role of the $(2 \times 2 \times 1)$ structure and chiral optical transitions: (i) The calculated circular polarization is finite and positive between ~520 and ~630 nm, and negative between ~630 and ~700 nm. In our measurements of TRCD [Fig. 1(b)] we find the chirality to be positive at 620 nm and negative at 680 nm, which coincides with our calculations of the sign of the chirality that we expect for both wavelengths. (ii) The order of magnitude of the circular dichroism between experiment and theory at these wavelengths is similar. This is also consistent with the range of wavelengths where finite circular polarization has been observed in previous studies of circular dichroism in $TiSe_2$ [2,19,25,28]. Note that this energy scale (1.8–2 eV) is much larger than the semiconducting gap (70 meV) of $TiSe_2$, so the typical DFT error in underestimating band gaps are of lesser importance in this range of energies.

We also conjecture that continuous wave excitation under sufficiently high power, long duration, and at lattice temperatures below T_{CDW}, as used in the study by Xu *et al.* [3], may also conspire to lead to the finite CPGE current. Based on our results and discussion presented above, this does not require the preexistence of chiral domains. Instead, photoexcitation above a critical power may lead to a finite fraction of the atomic structure being trapped in the noncentrosymmetric $P321$ structure, which would lead to finite chirality.

V. SUMMARY AND CONCLUSIONS

Hence, from these calculations we can conclude the following. The observation of chiral optical transitions during pump-probe measurements on $TiSe_2$ cannot be explained by the conventional $P\bar{3}c1$ structure that is associated with the $(2 \times 2 \times 2)$ commensurate CDW phase of $TiSe_2$. Instead, a

symmetry-breaking mechanism that leads to a finite difference between right and left circularly polarized optical transitions has to be operative. Our calculations suggest the noncentrosymmetric $P321$ structure that is near-degenerate in energy with the $P\bar{3}c1$ can be stabilized upon photoexcitation. The $P321$ structure leads to finite circularly polarized transitions that are consistent with the signatures of the chiral CDW that have been identified in pump-probe studies of $TiSe_2$.

The experimentally observed nonthermal melting of the CDW in $TiSe_2$, that is, melting of the CDW upon heating the electron subsystem, can be quantitatively explained by the effect of the electronic temperature on the electron screening of the ion-ion interactions. This is a one-electron effect not related in any manner with the physics of excitonic insulators. Therefore, nonthermal melting of the CDW alone does not provide evidence for the existence of an EI state in $TiSe_2$.

We also observe, in agreement with previous measurements, that the chiral optical response of $TiSe_2$ exists for a finite range of laser fluences, in other words, within a finite range of electronic temperatures. To this effect, we calculated the energy difference between the ground state centrosymmetric CDW structure ($P\bar{3}c1$) and the noncentrosymmetric $P321$ CDW structure, and found it to be extremely small (~5 K). Furthermore, this energy difference rapidly decreases as the electronic temperature increases. We conjecture that there is a small additional energy term, possibly related to vibrational entropy, that is outside the scope of our static lattice DFT calculations, which is either independent of the electronic temperature, or even grows with it. Such a contribution would impact the energy difference between the $P321$ and $P\bar{3}c1$ structures and lead to the noncentrosymmetric $P321$ structure to be the ground state at some intermediate electronic temperature. While this conjecture is purely speculative, it is consistent with the small and gradually decreasing energy difference between the chiral and achiral structures, and is in rather good agreement with the experimental observations.

[1] A. Kogar *et al.*, Signatures of exciton condensation in a transition metal dichalcogenide, Science **358**, 1314 (2017).

[2] T. Rohwer *et al.*, Collapse of long-range charge order tracked by time-resolved photoemission at high momenta, Nature (London) **471**, 490 (2011).

[3] S.-Y. Xu *et al.*, Spontaneous gyrotropic electronic order in a transition-metal dichalcogenide, Nature (London) **578**, 545 (2020).

[4] J. van Wezel, Chirality and orbital order in charge density waves, Europhys. Lett. **96**, 67011 (2011).

[5] M. Hellgren, J. Baima, R. Bianco, M. Calandra, F. Mauri, and L. Wirtz, Critical Role of the Exchange Interaction for the Electronic Structure and Charge-Density-Wave Formation in $TiSe_2$, Phys. Rev. Lett. **119**, 176401 (2017).

[6] K. Sugawara *et al.*, Unconventional charge-density-wave transition in monolayer $1T$-$TiSe_2$, ACS Nano **10**, 1341 (2016).

[7] F. Weber, S. Rosenkranz, J.-P. Castellan, R. Osborn, G. Karapetrov, R. Hott, R. Heid, K.-P. Bohnen, and A. Alatas, Electron-Phonon Coupling and the Soft Phonon Mode in TiSe₂, Phys. Rev. Lett. **107**, 266401 (2011).

[8] T. E. Kidd, T. Miller, M. Y. Chou, and T.-C. Chiang, Electron-Hole Coupling and the Charge Density Wave Transition in TiSe₂, Phys. Rev. Lett. **88**, 226402 (2002).

[9] K. Rossnagel, L. Kipp, and M. Skibowski, Charge-density-wave phase transition in 1*T*-TiSe₂: Excitonic insulator versus band-type Jahn-Teller mechanism, Phys. Rev. B **65**, 235101 (2002).

[10] H. Cercellier, C. Monney, F. Clerc, C. Battaglia, L. Despont, M. G. Garnier, H. Beck, P. Aebi, L. Patthey, H. Berger, and L. Forró, Evidence for an Excitonic Insulator Phase in 1*T*-TiSe₂, Phys. Rev. Lett. **99**, 146403 (2007).

[11] J. Ishioka, Y. H. Liu, K. Shimatake, T. Kurosawa, K. Ichimura, Y. Toda, M. Oda, and S. Tanda, Chiral Charge-Density Waves, Phys. Rev. Lett. **105**, 176401 (2010).

[12] M. Iavarone, R. Di Capua, X. Zhang, M. Golalikhani, S. A. Moore, and G. Karapetrov, Evolution of the charge density wave state in Cu$_x$TiSe₂, Phys. Rev. B **85**, 155103 (2012).

[13] C. Monney, C. Battaglia, H. Cercellier, P. Aebi, and H. Beck, Exciton Condensation Driving the Periodic Lattice Distortion of 1*T*-TiSe₂, Phys. Rev. Lett. **106**, 106404 (2011).

[14] H. Hughes, Structural distortion in TiSe₂ and related materials: A possible Jahn-Teller effect?, J. Phys. C: Solid State Phys. **10**, L319 (1977).

[15] M. H. Whangbo and E. Canadell, Analogies between the concepts of molecular chemistry and solid-state physics concerning structural instabilities: Electronic origin of the structural modulations in layered transition metal dichalcogenides, J. Am. Chem. Soc. **114**, 9587 (1992).

[16] J. van Wezel, P. Nahai-Williamson, and S. S. Saxena, Exciton-phonon-driven charge density wave in TiSe₂, Phys. Rev. B **81**, 165109 (2010).

[17] B. Zenker, H. Fehske, H. Beck, C. Monney, and A. R. Bishop, Chiral charge order in 1*T*-TiSe₂: Importance of lattice degrees of freedom, Phys. Rev. B **88**, 075138 (2013).

[18] E. Baldini *et al.*, The spontaneous symmetry breaking in Ta₂NiSe₅ is structural in nature, arXiv:2007.02909.

[19] E. Möhr-Vorobeva, S. L. Johnson, P. Beaud, U. Staub, R. De Souza, C. Milne, G. Ingold, J. Demsar, H. Schaefer, and A. Titov, Nonthermal Melting of a Charge Density Wave in TiSe₂, Phys. Rev. Lett. **107**, 036403 (2011).

[20] M. Burian, M. Porer, J. R. L. Mardegan, V. Esposito, S. Parchenko, B. Burganov, N. Gurung, M. Ramakrishnan, V. Scagnoli, H. Ueda, S. Francoual, F. Fabrizi, Y. Tanaka, T. Togashi, Y. Kubota, M. Yabashi, K. Rossnagel, S.L. Johnson, and U. Staub, Structural involvement in the melting of the charge density wave in 1*T*-TiSe₂, Phys. Rev. Res. **3**, 013128 (2021).

[21] B. Hildebrand, T. Jaouen, M.-L. Mottas, G. Monney, C. Barreteau, E. Giannini, D. R. Bowler, and P. Aebi, Local Real-Space View of the Achiral 1*T*-TiSe₂ $2 \times 2 \times 2$ Charge Density Wave, Phys. Rev. Lett. **120**, 136404 (2018).

[22] M.-K. Lin, J. A. Hlevyack, P. Chen, R.-Y. Liu, and T.-C. Chiang, Comment on "Chiral Phase Transition in

Charge Ordered 1*T*-TiSe₂", Phys. Rev. Lett. **122**, 229701 (2019).

[23] H. Ueda, M. Porer, J. R. L. Mardegan, S. Parchenko, N. Gurung, F. Fabrizi, M. Ramakrishnan, L. Boie, M. J. Neugebauer, B. Burganov, M. Burian, S. L. Johnson, K. Rossnagel, and U. Staub, Correlation between electronic and structural orders in 1*T*-TiSe₂, Phys. Rev. Res. **3**, L022003 (2021).

[24] Y. Peng, X. Guo, Q. Xiao, Q. Li, J. Strempfer, Y. Choi, D. Yan, H. Luo, Y. Huang, S. Jia *et al.*, Observation of orbital order in the van der Waals material 1*T*-TiSe₂, arXiv:2105.13195.

[25] C. W. Chuang, Y. Tanaka, M. Oura, K. Rossnagel, and A. Chainani, Attractive Coulomb interaction, temperature-dependent hybridization, and natural circular dichroism in 1*T*-TiSe₂, Phys. Rev. B **102**, 195102 (2020).

[26] J. E. Sipe and A. I. Shkrebtii, Second-order optical response in semiconductors, Phys. Rev. B **61**, 5337 (2000).

[27] L. Keldysh and Y. V. Kopaev, Possible instability of semimetallic state toward Coulomb interaction, Fiz. Tverd. Tela **6**, 2791 (1964) [Sov. Phys. Solid State **6**, 2219 (1965)].

[28] D. B. Lioi, Symmetry breaking in the correlated electronic and lattice degrees of freedom in the Cu$_x$TiSe$_x$*T-x* phase diagram, Ph.D. thesis, Drexel University, 2017.

[29] C. Lian, Z. A. Ali, and B. M. Wong, Charge density wave hampers exciton condensation in 1*T*-TiSe₂, Phys. Rev. B **100**, 205423 (2019).

[30] W. T. B. Kelvin, *The Molecular Tactics of a Crystal* (Clarendon Press, Oxford, 1894).

[31] F. J. Di Salvo, D. Moncton, and J. Waszczak, Electronic properties and superlattice formation in the semimetal TiSe₂, Phys. Rev. B **14**, 4321 (1976).

[32] P. E. Blöchl, Projector augmented-wave method, Phys. Rev. B **50**, 17953 (1994).

[33] G. Kresse and J. Hafner, *Ab initio* molecular dynamics for liquid metals, Phys. Rev. B **47**, 558 (1993).

[34] G. Kresse and J. Furthmüller, Efficient iterative schemes for *ab initio* total-energy calculations using a plane-wave basis set, Phys. Rev. B **54**, 11169 (1996).

[35] J. P. Perdew, K. Burke, and M. Ernzerhof, Generalized Gradient Approximation Made Simple, Phys. Rev. Lett. **77**, 3865 (1996).

[36] S. Grimme, J. Antony, S. Ehrlich, and H. Krieg, A consistent and accurate *ab initio* parametrization of density functional dispersion correction (DFT-D) for the 94 elements H–Pu, J. Chem. Phys. **132**, 154104 (2010).

[37] A. Togo and I. Tanaka, Spglib: A software library for crystal symmetry search, arXiv:1808.01590.

[38] C. A. Werley, S. M. Teo, and K. A. Nelson, Pulsed laser noise analysis and pump-probe signal detection with a data acquisition card, Rev. Sci. Instrum. **82**, 123108 (2011).

[39] See Supplemental Material at http://link.aps.org/supplemental/10.1103/PhysRevB.105.054102 for details of the electronic structure, approach to determine the degree of circular polarization from first principles, and convergence tests of the structural phase transition using different approximations within DFT; this supplementary material also contains Refs. [50–53].

[40] P. B. Allen, Theory of Thermal Relaxation of Electrons in Metals, Phys. Rev. Lett. **59**, 1460 (1987).

[41] T. Buslaps, R. Johnson, and G. Jungk, Spectroscopic ellipsometry on 1*T*-TiSe₂, Thin Solid Films **234**, 549 (1993).

[42] S. Bayliss and W. Liang, Reflectivity, joint density of states and band structure of group IVb transition-metal dichalcogenides, J. Phys. C: Solid State Phys. **18**, 3327 (1985).

[43] K. Velebit, P. Popčević, I. Batistić, M. Eichler, H. Berger, L. Forro, M. Dressel, N. Barisic, and E. Tutis, Scattering-dominated high-temperature phase of $1T$-TiSe$_2$: An optical conductivity study, Phys. Rev. B **94**, 075105 (2016).

[44] A. Wegner, D. Louca, and J. Yang, Local trigonal modes and the suppression of the charge density wave in TiSe$_{2-x}$Te$_x$, Phys. Rev. B **99**, 205110 (2019).

[45] A. Wegner, J. Zhao, J. Li, J. Yang, A. A. Anikin, G. Karapetrov, K. Esfarjani, D. Louca, and U. Chatterjee, Evidence for pseudo–Jahn-Teller distortions in the charge density wave phase of $1T$-TiSe$_2$, Phys. Rev. B **101**, 195145 (2020).

[46] M. D. Watson, A. M. Beales, and P. D. C. King, On the origin of the anomalous peak in the resistivity of TiSe$_2$, Phys. Rev. B **99**, 195142 (2019).

[47] J. M. Moya, C.-L. Huang, J. Choe, G. Costin, M. S. Foster, and E. Morosan, Effect of synthesis conditions on the electrical resistivity of TiSe$_2$, Phys. Rev. Mater. **3**, 084005 (2019).

[48] D. J. Campbell, C. Eckberg, P. Y. Zavalij, H. H. Kung, E. Razzoli, M. Michiardi, C. Jozwiak, A. Bostwick, E. Rotenberg, A. Damascelli, and J. Paglione, Intrinsic insulating ground state in transition metal dichalcogenide TiSe$_2$, Phys. Rev. Mater. **3**, 053402 (2019).

[49] M. D. Johannes and I. I. Mazin, Fermi surface nesting and the origin of charge density waves in metals, Phys. Rev. B **77**, 165135 (2008).

[50] C. Ambrosch-Draxl and J. O. Sofo, Linear optical properties of solids within the full-potential linearized augmented planewave method, Comput. Phys. Commun. **175**, 1 (2006).

[51] M. Maschek, S. Rosenkranz, R. Hott, R. Heid, M. Merz, D. A. Zocco, A. H. Said, A. Alatas, G. Karapetrov, S. Zhu, J. van Wezel, and F. Weber, Superconductivity and hybrid soft modes in TiSe$_2$, Phys. Rev. B **94**, 214507 (2016).

[52] K.-P. Bohnen, R. Heid, H. J. Liu, and C. T. Chan, Lattice Dynamics and Electron-Phonon Interaction in (3,3) Carbon Nanotubes, Phys. Rev. Lett. **93**, 245501 (2004).

[53] J. Heyd and G. E. Scuseria, Efficient hybrid density functional calculations in solids: Assessment of the Heyd-Scuseria-Ernzerhof screened Coulomb hybrid functional, J. Chem. Phys. **121**, 1187 (2004).